ADVANCED OPTICAL MATERIALS

www.advopticalmat.de

Designing the Iridescences of Biopolymers by Assembly of Photonic Crystal Superlattices

*Yu Wang, Meng Li, Elena Colusso, Wenyi Li, and Fiorenzo G. Omenetto**

Structural color in naturally occurring systems is generally constituted by nanoscale lattices of biopolymers that generate beautiful iridescences through their regular structures, often interspersed with defects or period mismatch. Taking inspiration from both formats and materials found in Nature, a series of large-scale, highly reflective biopolymer-based photonic crystal superlattices constituted by stacking layers of 3D nanoscale lattices with different periodicity is presented. These silk photonic crystal superlattices (SPCSs) are fully composed of naturally derived structural proteins (silk fibroin) and exhibit brilliant structural color while being mechanically flexible. Multi-stopbands over broad wavelength ranges or single-stopbands with narrowband spectral responses can be readily realized and precisely controlled by manipulating the hierarchy of the lattice stacks or the repetition periods of the assembled colloidal monolayers. The unique ability to vary the silk protein conformation allows to vary the lattice and controllably "design" the iridescences of the SPCSs with water vapor adding versatility to this biopolymer-based photonic structure.

Natural systems rely on ordered, quasi-ordered or disordered structural organizations with structural level over multiple length scales for the manipulation of light and the display of brilliant structural colors.[1] These complex hierarchical designs used in nature maximize their multifunctionality from a limited choice of available constituent elements. Biopolymers, such as chitin,[2] keratin,[3] cellulose,[4] and melanin,[5] are the primary self-assembling building blocks utilized by biological system to create such intricate architectures, which have provided inspiration for the fabrication of synthetic photonic materials that try to mimic their structure and optical features. However, regenerating nature-like complex photonic structure using natural building materials through a simple self-assembly process is still challenging.

Dr. Y. Wang, M. Li, E. Colusso, W. Li, Prof. F. G. Omenetto
Silklab
Department of Biomedical Engineering
Tufts University
Medford, MA 02155, USA
E-mail: Fiorenzo.Omenetto@tufts.edu
Prof. F. G. Omenetto
Department of Electrical Engineering
Tufts University
Medford, MA 02155, USA
Prof. F. G. Omenetto
Department of Physics
Tufts University
Medford, MA 02155, USA

DOI: 10.1002/adom.201800066

Photonic crystals (PhCs), especially 3D colloidal PhCs or their inverse replica materials (inverse opals), have emerged as attractive optical materials to selectively control the flow of light and to generate bright iridescences through the definition of photonic bandgaps (PBGs).[6,7] The common colloidal PhCs are homogeneous 3D periodic structures formed from monodisperse colloids, which have been widely investigated.[8,9] Recently, 3D colloidal photonic crystal heterostructures fabricated through combining spheres of different size have also attracted considerable interest owing to their special optical properties,[10–14] such as the existence of multiple stopbands and high reflectivity over broad wavelength ranges, and the resulting potential applications in broadband back-reflectors,[13] electrodes in solar cells,[15] thermal barrier coatings,[16] optical filters,[17] and sensing.[18] So far, a variety of techniques, including convective self-assembly,[19] Langmuir–Blodgett (LB) technique,[20] vertical deposition,[21] layer-by-layer transfer,[13] and controlled dip-coating[22] as well as the combination of these techniques with atomic layer deposition,[14] and electrodeposition,[11] have been developed to fabricate colloidal PhCs heterostructures with different forms, such as, multilayer opaline heterostructures,[10,14] sandwich-like colloidal crystals,[23,24] and colloidal PhC superlattices.[13,25]

Unlike naturally occurring photonics crystals, colloidal PhCs heterostructures are typically fabricated from inorganic constituents or synthetic polymer. Bringing the techniques of sophisticated defect engineering to biopolymers not only makes them approach the hierarchy of naturally occurring structures but also adds an array of opportunities for embedding sophisticated optical control into biomaterials. In this work, we use naturally derived materials, specifically silk fibroin, to realize colloidal PhC heterostructures that can generate tunable structural color in a mechanically flexible and tunable format. In contrast to their inorganic counterparts, we show that these protein-based superlattices can still change conformation and "evolve" the stopbands and the defects. Additionally, the ability to control and design spectral responses in a biomaterial also extends the utility of colloidal heterostructures to biological applications such as high reflection-based or label-free biosensing.[18,26,27]

Silk fibroin, collected from the domesticated *Bombyx mori* silkworm, has been regarded as a promising candidate for biocompatible optics, bioresorbable photonics, implantable and biofunctional optical devices because of its excellent combination

 © 2018 WILEY-VCH Verlag GmbH & Co. KGaA, Weinheim

of biocompatibility, biodegradability, and high transparency.[28,29] Thanks to its water-based suspension, mild processing conditions, nanoscale processability, and mechanical durability,[30] silk fibroin has been structured by a variety of fabrication strategies to design different optical elements including photonic crystals,[31–33] lenses,[34] 2D microprism arrays,[35] diffraction gratings,[36,37] waveguides,[38,39] high-Q resonators,[40] and lasers.[41,42] More importantly, silk fibroin materials can be easily functionalized through simple mixing of inorganic or organic dopants in the water solution and casting process, maintaining the activity and functions of the entrapped dopants.[43]

We demonstrate here the construction of biopolymer-based photonic crystal heterostructures as well as the ability to design the stopband and to reconfigure the lattice of the formed heterostructure to further tune the spectral response of the material. This comprises (a) the preparation of large-scale (i.e., centimeter length scales), flexible silk photonic crystal superlattices (SPCSs) with different architectures (b) the design of structural color and stopbands of SPCSs through variations in the alternating lattice stacks and repetition periods, and (c) reconfiguration of the superlattices by controlling the silk fibroin protein conformation and reorientation on the nanoscale with water vapor (WV).

The SPCSs are obtained from a polystyrene (PS) colloidal PhC superlattice formed through layer-by-layer stacking of colloidal monolayers based on the use of PS nanospheres with two different sizes. The fabrication procedure is shown in **Figure 1**. First, large-scale colloidal monolayers with nanosphere diameters of 300 nm (A^o) and 210 nm (B^o) are separately assembled at the water–air interface (see Figure S1a, Supporting Information) after the nanospheres are introduced onto the water surface (Figure 1i,ii). The resulting close-packed PS sphere monolayers (of sizes A^o and B^o) are then transferred and stacked in a desired order (Figure 1iii), resulting in a large-area PS colloidal crystal superlattice onto a silicon substrate. After the template preparation, aqueous silk solution extracted from *B. mori* silkworm cocoons is poured onto the template and allowed to solidify into an amorphous silk/PS composite film. The SPCS is then obtained by immersing the composite film into toluene to dissolve the PS spheres. The resulting freestanding SPCSs exhibit excellent mechanical properties and are flexible,[44] guaranteeing their potential applications both in wet and dry environments.

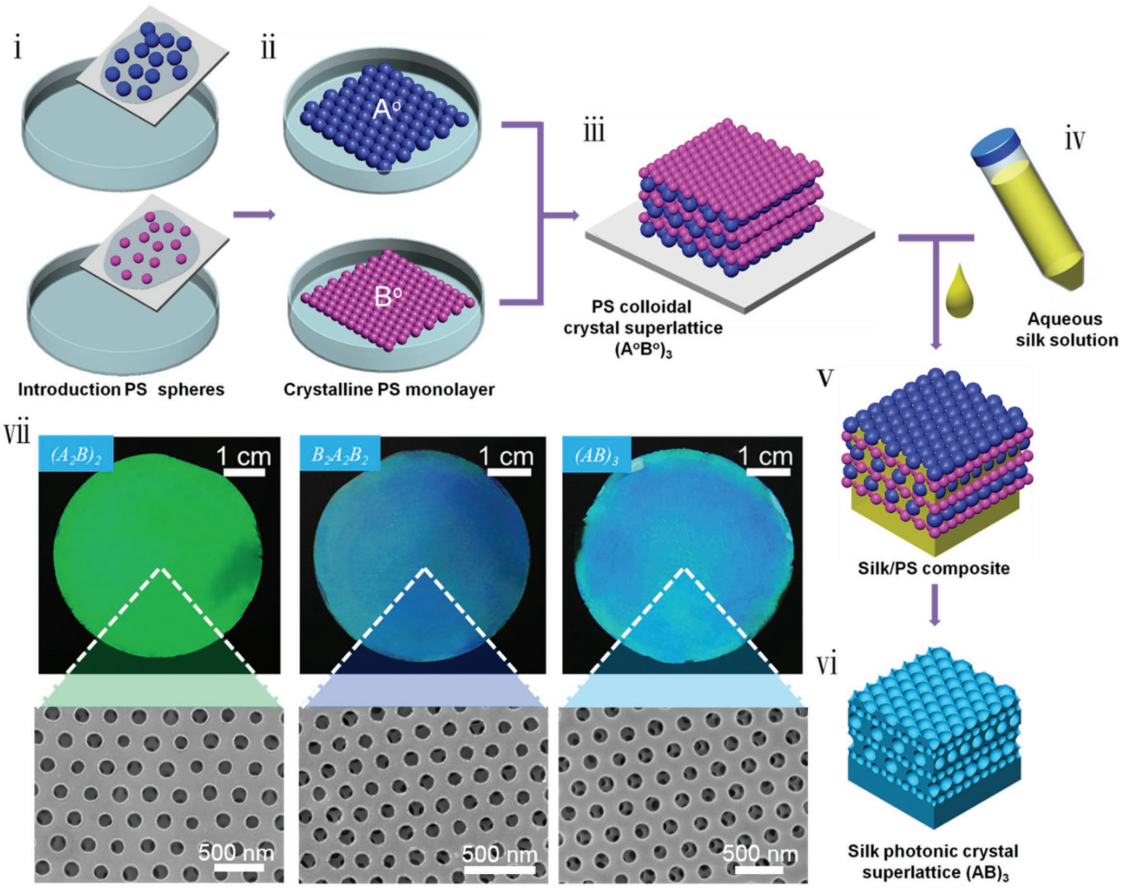

Figure 1. Fabrication process for large-scale silk photonic crystal superlattice $(AB)_3$. i) Monodisperse PS spheres are introduced onto the water surface using a hydrophilic substrate. The different colors represent PS spheres with different size. ii) The PS spheres self-assemble and form a close-packed monolayer at the water/air interface. iii) PS colloidal monolayers A^o and B^o are alternatingly transferred from the water/air interface to the substrate to form the PS colloidal crystal superlattice in a $(AB)_3$ arrangement. iv) Aqueous silk solution is obtained from the cocoons of the *B. mori* silkworm. v) The free-standing silk/PS composite film is obtained by infiltrating the PS template with silk solution and drying. vi) Silk photonic crystal superlattice $(AB)_3$ is formed by immersing the composite film into toluene to dissolve the PS spheres. vii) Photographs and the corresponding surface SEM images of three SPCSs with different stacking rules: $(A_2B)_2$ (left), $B_2A_2B_2$ (middle), $(AB)_3$ (right).

© 2018 WILEY-VCH Verlag GmbH & Co. KGaA, Weinheim

To demonstrate the versatility of this approach, six-layer SPCSs are assembled with different stacking orders using the strategy described above. The structures are represented as A_n, B_n with A and B referring to the pitch of the lattice (A = 300 nm and B = 210 nm) and with the subscript n representing the number of layers in the stack. Large-scale (≈5 cm in diameter), flexible, and macro defect free SPCSs with vivid structural colors are obtained (Figure 1vii). The top-view scanning electron microscopy (SEM) images of the three typical SPCSs show the highly ordered hexagonal arrays of air cavities (where the PS spheres were originally located) over a large area. The center-to-center distance of the air cavities in each layer defines the lattice constant Λ and corresponds to each diameter of PS sphere used (i.e., 210 and 300 nm), respectively. Underneath the top air cavities, "triangular" lattice structures can be seen to illustrate the presence of the photonic crystal lattice. It must be noted that disorder is introduced in the lattice because of the size mismatch in between the different size nanospheres that come into contact during structure formation.

Figure 2 shows the cross-sectional images and the reflectance spectra of all the six-layer SPCSs. The ordered hollow silk fibroin structure with air holes on the wall, and the different stacking hierarchies can be clearly seen from all the cross-sectional images. The total reflectance spectrum from the SPCS structures is measured using a spectrophotometer combined with an integrating sphere. Distinct iridescences (i.e., structural colors) are generated by employing different stacking patterns of A and B monolayers. The SPCS with A_3B_3 arrangement shows a broad stopband ranging from 375 to 700 nm (Figure 2a) with three distinguished reflection peaks located at 410, 490, and 595 nm, respectively.

The peaks around 410 and 595 nm correspond to the stopbands of the respective silk inverse opal (SIO) layers, as seen in Figure S2 (Supporting Information). The new peak located at 490 nm is believed to be the results of the superposition of the two adjacent stopbands because of their strong interaction at the interface,[45] which is further corroborated by the absence of a clear interface between the two SIO layers. For the $(AB)_3$ arrangement (Figure 2b), the primary reflection peaks of the silk photonic crystal merge into a narrow peak centered at 490 nm due to the strong interaction between the A and B monolayers. As for $A_2B_2A_2$, three separate reflectance peaks located at 380, 500, and 640 nm can be detected (Figure 2c), and for $B_2A_2B_2$, two reflectance peaks located at 390 and 480 nm are identified (Figure 2d). In these cases, the middle B_2 or A_2 layers behaves as an optical cavity, resulting in a pronounced dip (passband) inside the original stopband of the corresponding inverse opal (Figure S2, Supporting Information). It should also be mentioned that the detected peak at 380 nm in $A_2B_2A_2$ might arise from the interaction between the uppermost A_2 and B_2 layers. In the case of $(A_2B)_2$ or $(AB_2)_2$ arrangement (Figure 2e,f), like in the $(AB)_3$ arrangement, a narrow peak is detected with center wavelength at 520 or 460 nm, respectively. It can be concluded that the different periodicities of SPCSs bring about significant modifications to the stopbands, which can not only generate multiple stopbands over broad wavelength ranges (Figure 2a,c,d), but also generate a single stopband with high reflectivity and narrow bandwidth (Figure 2b,e,f).

The optical properties of the SPCSs can be affected by the stacking sequence, as shown in Figure S3 (Supporting Information). Compared to the A_3B_3 arrangement, the B_3A_3 arrangement shows only two isolated reflectance peaks corresponding

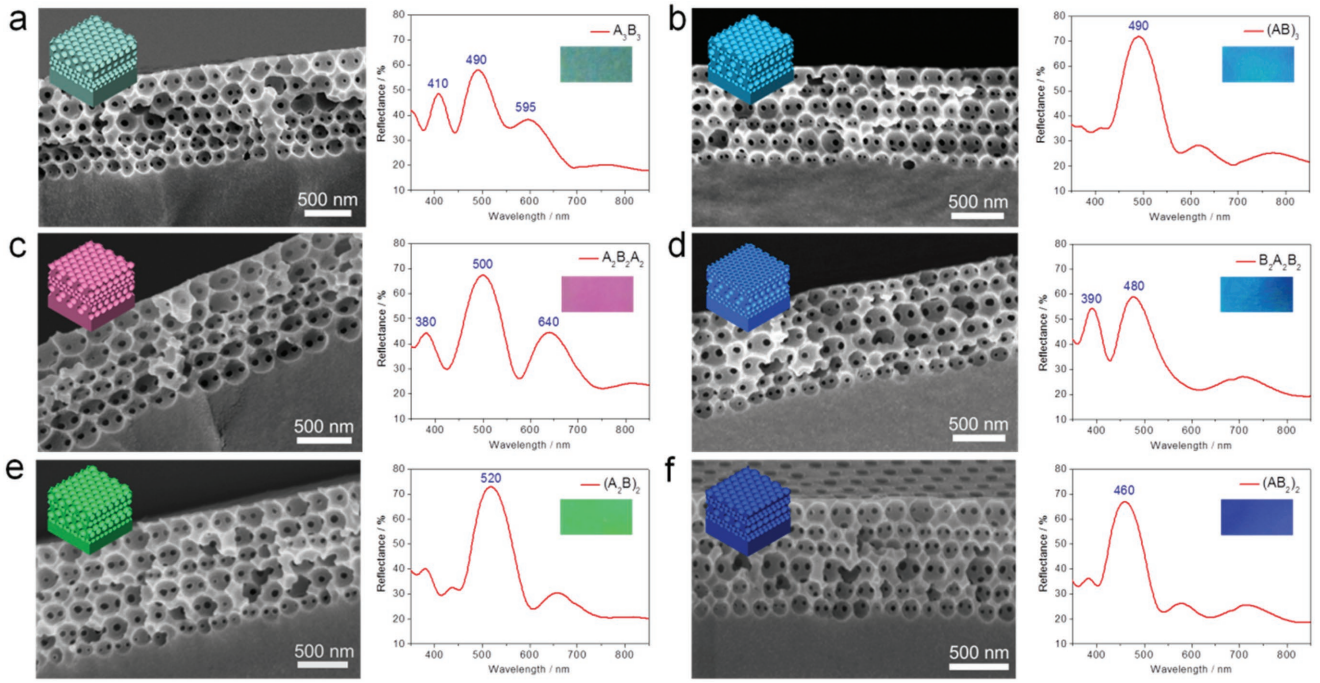

Figure 2. Cross-sectional SEM images (left) and total reflectance spectra (right) of SPCSs. a) A_3B_3, b) $(AB)_3$, c) $A_2B_2A_2$, d) $B_2A_2B_2$, e) $(A_2B)_2$, f) $(AB_2)_2$. The peak position is presented near the corresponding peak. Inserts: schematic illustration and photograph of the corresponding photonic crystal superlattice.

© 2018 WILEY-VCH Verlag GmbH & Co. KGaA, Weinheim

to the stopbands of the respective SIO layers, which are attributed to the weak interface interaction between the two SIO layers. Since the holes are a replica of the PS spheres used as the template during the formation process of this SPCS, this result indicates that larger spheres stacking on the smaller spheres can form flat and well-defined interfaces and avoid significant interface irregularities, compared to the case of smaller spheres stacked on the larger spheres.[46] As for $(BA)_3$, $(BA_2)_2$, and $(B_2A)_2$, the intensity of the reflectance peak attenuates slightly and the Fabry–Perot fringes (indicated by arrows) that result from the reflections at the front and rear facets of the samples[47] appear (on the left side of the reflectance peak) or disappear (on the right side of the reflectance peak), compared to their opposing arrangement.

The influence of the repetition periods on the optical properties of a series of SPCSs with different stacking orders ($(AB)_n$, $(A_2B)_n$, A_nB_n, A_nBA_n, $A_nB_nA_n$, and $A_2B_nA_2$) was also investigated. The results are illustrated in **Figure 3**. Although all the SPCSs exhibit higher intensity and narrower spectral bandwidth in the stopband with increasing period number, there are significant differences for SPCSs with different stacking orders. As shown in Figure 3a,b, the position of the stopband is constant with the period number increasing for $(AB)_n$ stacking order, but it is gradually blue-shifted for $(A_2B)_n$ stacking order. For these two arrangements, the reflectance spectra exhibit more obvious superlattice features with more Fabry–Perot fringes that appear with the increase of the period number. As for A_nB_n or A_nBA_n arrangement, the position of a peak located at 490 or 525 nm stay unchanged, while the peaks located on either side shift closer to this peak as the period number is increased (Figure 3c,d). In the case of $A_nB_nA_n$ or $A_2B_nA_2$ arrangements, the number of stopbands increases with increasing period number and the main stopband is gradually blue-shifted. For example, the $A_2B_4A_2$ exhibits four isolated stopbands with narrow width ranging from 350 to 755 nm, which enable high reflectivity over broad wavelength ranges. These results indicate that the stopbands (and structural colors, see Figure S4, Supporting Information) of SPCSs can also be largely tuned by the repetition periods, where significant modifications can arise from the increased long-range periodicity of the superlattice or the increased interaction between the A_n and B_n with the increase of period number.

We also explored the angle dependence of the specular reflectance spectra of all the six-layer SPCSs. As shown in **Figure 4**, the reflection peaks of all the samples shift to shorter wavelength gradually when the incident angle changes from 20° to 45° with respect to the film normal. The spectral shift trend is similar for all the SPCSs as well as the SIO obtained from 300 nm PS spheres (Figure S5a, Supporting Information). Analysis of the spectra of SPCSs with multiple stopbands (such as A_3B_3) and those with single stopband (such as $(AB_2)_2$) reveals that the spectra of the A_3B_3 arrangement display a large degree of overlap when the incident angle varies from 20° to 45° (Figure 4a or see also Figure S5b, Supporting Information) compared to those of $(AB_2)_2$ arrangement (Figure 4f or see also Figure S5c, Supporting Information). Such kind of SPCS might find potential application for broad range reflection of light at different incident angles, such as in broad-spectrum solar cells.[48]

It was recently shown that WV can modulate the stopband (and the structural color) of amorphous SIO by varying the conformation of the silk protein and, consequently, inducing controllable anisotropic shrinkage of the photonic lattices.[44] The optical response of six-layer SPCSs to water vapor was investigated here. As shown in **Figure 5**a, the structural color

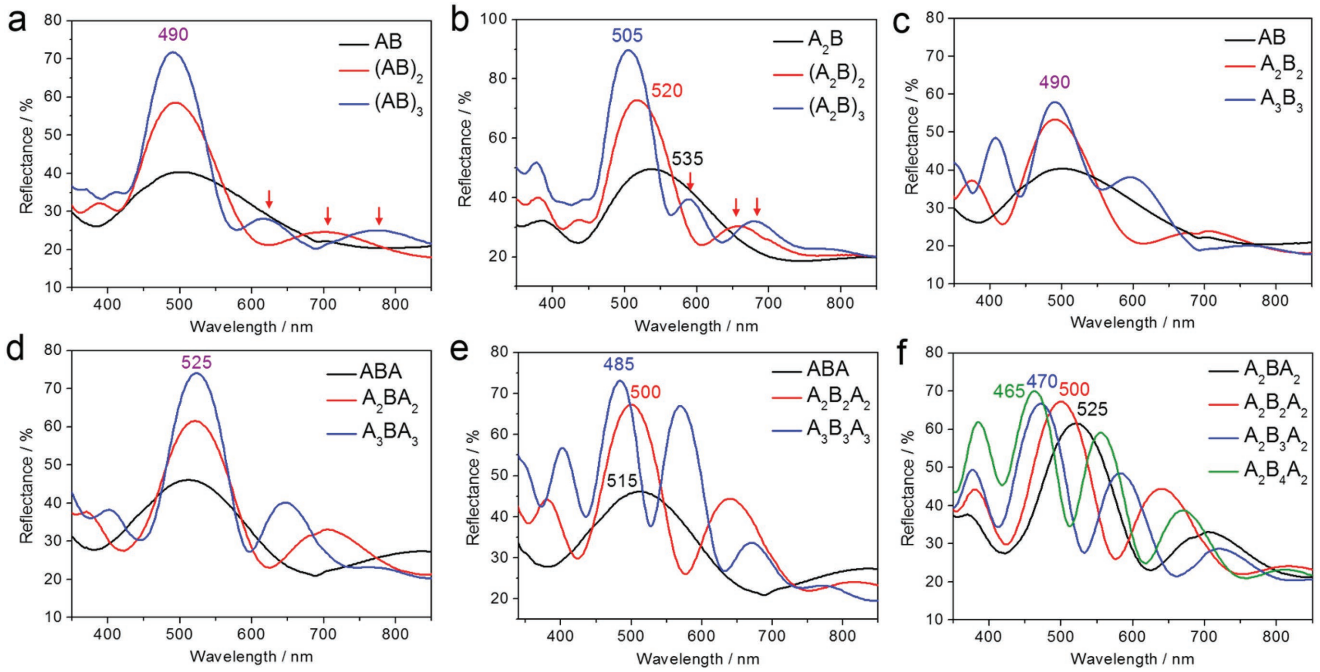

Figure 3. The total reflectance spectra of SPCSs with different repetition periods. a) $(AB)_n$, b) $(A_2B)_n$, c) A_nB_n, d) A_nBA_n, e) $A_nB_nA_n$, f) $A_2(B_n)A_2$. $n = 1$, 2, and 3 for (a–e), $n = 1$, 2, 3, and 4 for (f). The arrows in (a) and (b) indicate the Fabry–Perot fringes.

© 2018 WILEY-VCH Verlag GmbH & Co. KGaA, Weinheim

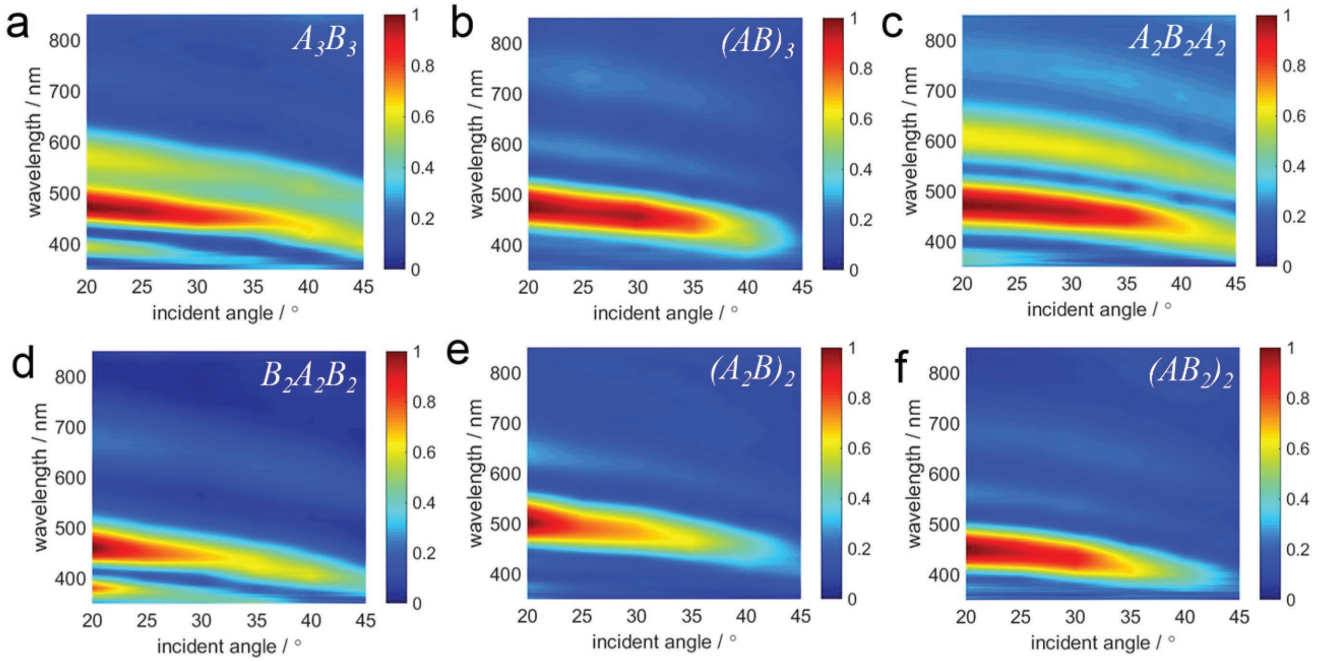

Figure 4. Angle dependence of optical properties. Wavelength as a function of incident angle of six-layer SPCSs with different arrangements. a) A_3B_3, b) $(AB)_3$, c) $A_2B_2A_2$, d) $B_2A_2B_2$, e) $(A_2B)_2$, f) $(AB_2)_2$. The stopbands are gradually blue-shifted with the detection angles.

and, thus, the lattices of all the six-layer SPCSs can be tuned and are reconfigured by WV treatment. The corresponding stopband shifts are shown in Figure 5b–g. As for the SPCS with multi-stopband (Figure 5b,d,e), all the reflectance peaks are gradually blue-shifted and the stopband in the short wavelength gradually becomes invisible with increasing the WV treatment time, resulting in the unique structural color change shown in Figure 5a. As can be seen from Figure 5e, the main reflectance peaks disappear after WV treatment for six times and the structural color is dominated by the small and broad Fabry–Perot fringes. A similar phenomenon is also observed for $(AB_2)_2$ stacks (Figure 5g). These blue-shifted stopbands (or structural colors) are attributed to the compression of the superlattices along the vertical direction of the SPCS films due to the molecular chains rearrangement during conformational change (from random coil or helix to beta-sheet) of the amorphous silk format induced by WV.[44] Such induced structural changes are irreversible, similarly to the case of amorphous

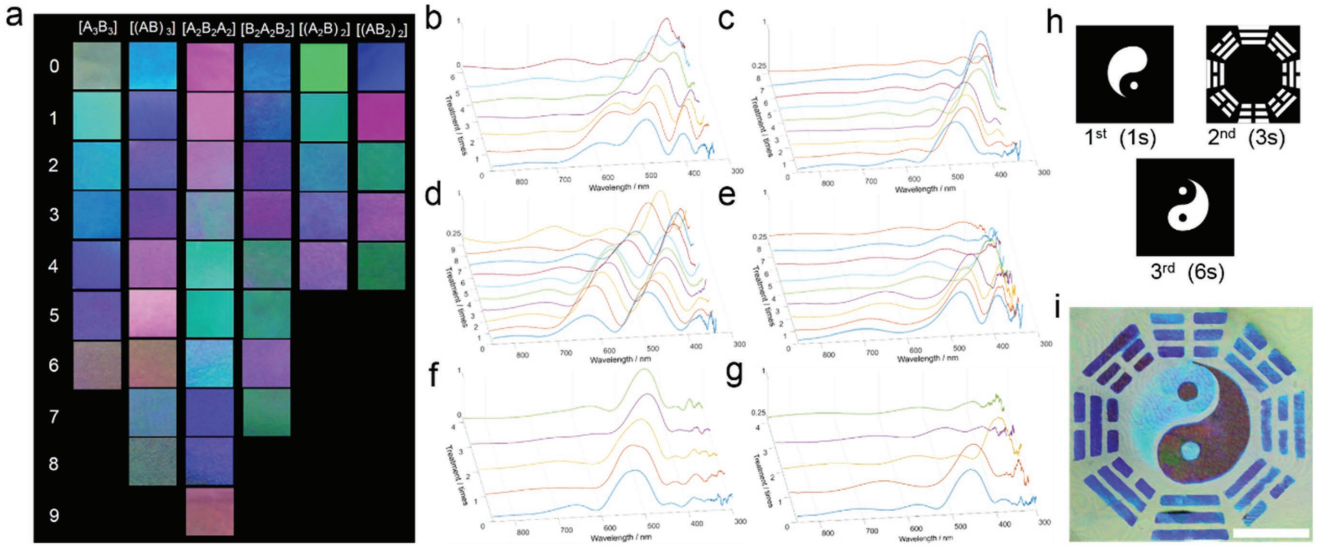

Figure 5. Optical response of SPCSs to water vapor. a) A series of photographs of SPCSs as a function of different treatment times of water vapor. b–g) Normalized specular reflectance spectra of water vapor-treated SPCSs: b) A_3B_3, c) $(AB)_3$, d) $A_2B_2A_2$, e) $B_2A_2B_2$, f) $(A_2B)_2$, g) $(AB_2)_2$. The reflectance peaks are gradually blue-shifted with the increase of treating time. h) Three different stencil designs used to create a Bagua pattern on the A_3B_3 stacked SPCS by selectively exposing part of SPCS to water vapor for different times. i) The corresponding photograph of patterned SPCS. Scale bar: 5 mm.

© 2018 WILEY-VCH Verlag GmbH & Co. KGaA, Weinheim

SIOs.[44] Besides, it should be mentioned that the refractive index of the SPCSs is almost unchanged after WV treatment. The controllable variation of the structural color by WV enables the design of multispectral patterns on SPCSs by using different stencils to selectively expose part of SPCS to WV for different times. For example, the Chinese Bagua pattern was prepared with a size of 1.5×1.5 cm^2, and three different stencils were used for each of the sequential WV exposure steps (Figure 5h). Based on this, a multispectral photonic crystal superlattice can be generated from an A_3B_3 stacking arrangement, as shown in Figure 5i.

In summary, we have successfully designed a series of cm length scale, highly reflective silk photonic crystal superlattices with multiple stacking orders and lattice periods. The SPCSs display bright structural color and are highly flexible due to the robust mechanical properties of silk. The SPCSs show either multi-stopband over broad wavelength ranges or single-stopbands with narrow bandwidths. The structures are highly tunable through programmable ordering of stacks and repetition periods, allowing refined control of the structure iridescences and color responses. The structural colors of such SPCSs can be reconfigured and rationally designed by "contact-free" water vapor exposure thanks to the ability of amorphous silk format to change its conformation on the nanoscale. The high reflectivity, ability to design and process SPCSs offers promising opportunities in multiple applications, such as tunable broadband photonic reflectors for energy applications, biosensing, low-threshold lasing, or custom optical filters, that exploit structural proteins and recapitulate the iridescences that are found in Nature, expanding on their utility.

Experimental Section

Silk Solution Preparation: The aqueous silk solution was prepared as previously described.[30] Briefly, *B. mori* silk cocoons were cut in small pieces and boiled for 30 min in a 0.02 M Na_2CO_3 water solution to remove the sericin. After washing with deionized water and then drying for 2 d, the degummed silk fibers were dissolved in 9.3 M LiBr solution at 60 °C for 4 h, followed by dialysis against deionized water using a dialysis tube (Fisherbrand, MWCO 3.5K) for 3 d to obtain a 7–8 wt% silk fibroin solution in water.

Silk Photonic Crystal Superlattice Preparation: The SPCS was prepared by using large-scale PS colloidal crystal superlattice as template. The close-packed PS nanosphere monolayer on the water surface was prepared according to the method described in detail elsewhere.[44,49–52] Briefly, 30 µL monodisperse PS sphere suspension were introduced to the water surface by using the partially immersed hydrophilic Si wafer as transferring substrate. After removing the spheres immersed into the subphase of water and extra adding a few drops of sodium dodecyl sulfate (SDS), the PS spheres formed a large-scale close-packed monolayer array on the water surface. To fabricate the PS colloidal crystal superlattice structure, crystalline PS monolayer arrays with two different diameters (300 and 210 nm) on the water surface were prepared respectively in different containers, then, according to a designed stacking order (taking $(A°B°)_3$ for example), the Si substrate was first immersed into the subphase of the colloidal monolayer ($A°$) and elevated under a shallow angle to transfer the monolayer. After dried, this silicon substrate with monolayer $A°$ was inserted into the subphase of the colloidal monolayer ($B°$) and lifted off to transfer this monolayer. Thus, the first repeat unit ($A°B°$) of superlattice was completed. Then, PS colloidal crystal superlattice could be obtained by repeating this unit for three times. After preparing the template, the silk solution was added to the colloidal crystal superlattice to fill the air voids. The sample was set to dry for 24 h (25 °C, 30% relative humidity) to form a free-standing silk/PS composite film with the thickness of about 50 µm. The SPCS with $(AB)_3$ arrangement was finally obtained by immersing the composite film into toluene for 24 h to remove all the PS spheres.

Water Vapor Treatment: Water vapor treatment was carried out by placing the SPCSs on top of the heated water surface (about 40 °C) with the nanostructured surface of SPCSs directly exposed to water vapor for 1 s each time. This treatment was finished until no color change was induced by water vapor. The distance between sample and water surface was set as 5 mm. For patterned SPCS, Stencils with various designs and sizes were applied on the surface of SPCS film before water vapor treatment to leave desired pattern on it after mask removal.

Measurement: FESEM was used to observe the surface and cross-sectional morphology of SPCS films. To analyze the cross-sectional structure, the samples were cleaved via cryofracture. All samples were sputtered with a 5 nm thick layer of gold using an EMS 300T D Dual Head Sputter Coater before being observed under a Zeiss Supra55VP with secondary electrons at 5 kV.

The total reflectance spectra of all SPCSs were collected using a UV–vis–NIR spectrometer (V-570, Jasco) with an integrating sphere (ISV-469, Jasco). The specular reflectance spectra were recorded using a fiber-optic spectrometer (USB-2000, OceanOptics).

Supporting Information

Supporting Information is available from the Wiley Online Library or from the author.

Acknowledgements

The authors acknowledge support from the Office of Naval Research grant (N00014-16-1-2437) for this work.

Conflict of Interest

The authors declare no conflict of interest.

Keywords

conformational control, iridescences, manipulable lattices, photonic crystal superlattices, silk fibroin

Received: January 18, 2018
Revised: February 7, 2018
Published online:

[1] P. Vukusic, J. R. Sambles, *Nature* **2003**, *424*, 852.
[2] D. Zhang, W. Zhang, J. J. Gu, T. X. Fan, Q. L. Liu, H. L. Su, S. M. Zhu, *Prog. Mater. Sci.* **2015**, *68*, 67.
[3] J. Zi, X. D. Yu, Y. Z. Li, X. H. Hu, C. Xu, X. J. Wang, X. H. Liu, R. T. Fu, *Proc. Natl. Acad. Sci. USA* **2003**, *100*, 12576.
[4] S. Vignolini, P. J. Rudall, A.V. Rowland, A. Reed, E. Moyroud, R. B. Faden, J. J. Baumberg, B. J. Glover, U. Steiner, *Proc. Natl. Acad. Sci. USA* **2012**, *109*, 15712.
[5] C. M. Eliason, M. D. Shawkey, *J. R. Soc. Interface* **2012**, *9*, 2279.
[6] J. D. Joannopoulos, P. R. Villeneuve, S. H. Fan, *Nature* **1997**, *386*, 143.
[7] S. Noda, K. Tomoda, N. Yamamoto, A. Chutinan, *Science* **2000**, *289*, 604.

© 2018 WILEY-VCH Verlag GmbH & Co. KGaA, Weinheim

[8] Y. N. Xia, B. Gates, Y. D. Yin, Y. Lu, *Adv. Mater.* **2000**, *12*, 693.
[9] K. R. Phillips, G. T. England, S. Sunny, E. Shirman, T. Shirman, N. Vogel, J. Aizenberg, *Chem. Soc. Rev.* **2016**, *45*, 281.
[10] P. Jiang, G. N. Ostojic, R. Narat, D. M. Mittleman, V. L. Colvin, *Adv. Mater.* **2001**, *13*, 389.
[11] M. Heim, S. Reculusa, S. Ravaine, A. Kuhn, *Adv. Funct. Mater.* **2012**, *22*, 538.
[12] Z. Cai, Y. J. Liu, J. Teng, X. Lu, *ACS Appl. Mater. Interfaces* **2012**, *4*, 5562.
[13] L. Zhang, Z. Xiong, L. Shan, L. Zheng, T. Wei, Q. Yan, *Small* **2015**, *11*, 4910.
[14] R. Kubrin, R. M. Pasquarelli, M. Waleczek, H. S. Lee, R. Zierold, J. J. do Rosario, P. N. Dyachenko, J. M. Montero Moreno, A. Y. Petrov, R. Janssen, M. Eich, K. Nielsch, G. A. Schneider, *ACS Appl. Mater. Interfaces* **2016**, *8*, 10466.
[15] A. Mihi, M. Calvo, J. Anta, H. Miguez, *J. Phys. Chem. C* **2008**, *112*, 13.
[16] H. S. Lee, R. Kubrin, R. Zierold, A. Y. Petrov, K. Nielsch, G. A. Schneider, M. Eich, *J. Opt. Soc. Am. B* **2012**, *29*, 450.
[17] F. Fleischhaker, A. C. Arsenault, V. Kitaev, F. C. Peiris, G. von Freymann, I. Manners, R. Zentel, G. A. Ozin, *J. Am. Chem. Soc.* **2005**, *127*, 9318.
[18] C. Fenzl, T. Hirsch, O. S. Wolfbeis, *Angew. Chem., Int. Ed.* **2014**, *53*, 3318.
[19] R. V. Nair, R. Vijaya, *J. Appl. Phys.* **2007**, *102*, 056102.
[20] M. Bardosova, M. E. Pemble, I. M. Povey, R. H. Tredgold, D. E. Whitehead, *Appl. Phys. Lett.* **2006**, *89*, 093116.
[21] S. Wong, V. Kitaev, G. A. Ozin, *J. Am. Chem. Soc.* **2003**, *125*, 15589.
[22] M. Egen, R. Voss, B. Griesebock, R. Zentel, *Chem. Mater.* **2003**, *15*, 3786.
[23] K. Wostyn, Y. Zhao, G. de Schaetzen, L. Hellemans, N. Matsuda, K. Clays, A. Persoons, *Langmuir* **2003**, *19*, 4465.
[24] Y. Zhao, K. Wostyn, G. de Schaetzen, K. Clays, L. Hellemans, A. Persoons, M. Szekeres, R. A. Schoonheydt, *Appl. Phys. Lett.* **2003**, *82*, 3764.
[25] R. Rengarajan, P. Jiang, D. C. Larrabee, V. L. Colvin, D. M. Mittleman, *Phys. Rev. B* **2001**, *64*, 205103.
[26] M. Fujishima, S. Sakata, T. Iwasaki, K. Uchida, *J. Mater. Sci.* **2008**, *43*, 1890.
[27] H. Inan, M. Poyraz, F. Inci, M. A. Lifson, M. Baday, B. T. Cunningham, U. Demirci, *Chem. Soc. Rev.* **2017**, *46*, 366.
[28] F. G. Omenetto, D. L. KapLan, *Nat. Photonics* **2008**, *2*, 641.
[29] T. Scheibel, A. Leal-Egana, *Biotechnol. Appl. Biochem.* **2010**, *55*, 155.
[30] H. Tao, D. L. Kaplan, F. G. Omenetto, *Adv. Mater.* **2012**, *24*, 2824.
[31] S. Kim, A. N. Mitropoulos, J. D. Spitzberg, H. Tao, D. L. Kaplan, F. G. Omenetto, *Nat. Photonics* **2012**, *6*, 817.
[32] Y. Y. Diao, X. Y. Liu, G. W. Toh, L. Shi, J. Zi, *Adv. Funct. Mater.* **2013**, *23*, 5373.
[33] K. Mina, S. Kim, S. Kim, *Proc. Natl. Acad. Sci. USA* **2017**, *114*, 6185.
[34] B. D. Lawrence, M. Cronin-Golomb, I. Georgakoudi, D. L. Kaplan, F. G. Omenetto, *Biomacromolecules* **2008**, *9*, 1214.
[35] H. Tao, J. M. Kainerstorfer, S. M. Siebert, E. M. Pritchard, A. Sassaroli, B. J. B. Panilaitis, M. A. Brenckle, J. J. Amsden, J. Levitt, S. Fantini, D. L. Kaplan, F. G. Omenetto, *Proc. Natl. Acad. Sci. USA* **2012**, *109*, 19584.
[36] J. J. Amsden, P. Domachuk, A. Gopinath, R. D. White, L. Dal Negro, D. L. Kaplan, F. G. Omenetto, *Adv. Mater.* **2010**, *22*, 1746.
[37] Z. T. Zhou, Z. F. Shi, X. Q. Cai, S. Q. Zhang, S. G. Corder, X. X. Li, Y. S. Zhang, G. Z. Zhang, L. Chen, M. K. Liu, D. L. Kaplan, F. G. Omenetto, Y. Mao, Z. D. Tao, T. H. Tao, *Adv. Mater.* **2017**, *29*, 1605471.
[38] S. T. Parker, P. Domachuk, J. Amsden, J. Bressner, J. A. Lewis, D. L. Kaplan, F. G. Omenetto, *Adv. Mater.* **2009**, *21*, 2411.
[39] H. Guerboukha, G. F. Yan, O. Skorobogata, M. Skorobogatiy, *Adv. Opt. Mater.* **2014**, *2*, 1181.
[40] L. H. Xu, X. F. Jiang, G. M. Zhao, D. Ma, H. Tao, Z. W. Liu, F. G. Omenetto, L. Yang, *Opt. Express* **2016**, *24*, 20825.
[41] Y. Choi, H. Jeon, S. Kim, *Lab Chip* **2015**, *15*, 642.
[42] S. Caixeiro, M. Gaio, B. Marelli, F. G. Omenetto, R. Sapienza, *Adv. Opt. Mater.* **2016**, *4*, 998.
[43] E. M. Pritchard, P. B. Dennis, F. Omenetto, R. R. Naik, D. L. Kaplan, *Biopolymers* **2012**, *97*, 479.
[44] Y. Wang, D. Aurelio, W. Y. Li, P. Tseng, Z. Z. Zheng, M. Li, D. L. Kaplan, M. Liscidini, F. G. Omenetto, *Adv. Mater.* **2017**, *29*, 1702769.
[45] Q. Yan, L. K. Teh, Q. Shao, C. C. Wong, Y. M. Chiang, *Langmuir* **2008**, *24*, 1796.
[46] M. Bardosova, M. E. Pemble, I. M. Povey, R. H. Tredgold, D. E. Whitehead, *Appl. Phys. Lett.* **2006**, *89*, 093116.
[47] P. Masse, G. Pouclet, S. Ravaine, *Adv. Mater.* **2008**, *20*, 584.
[48] P. G. O'Brien, N. P. Kherani, A. Chutinan, G. A. Ozin, S. John, S. Zukotynski, *Adv. Mater.* **2008**, *20*, 1577.
[49] M. Retsch, Z. C. Zhou, S. Rivera, M. Kappl, X. S. Zhao, U. Jonas, Q. Li, *Macromol. Chem. Phys.* **2009**, *210*, 230.
[50] N. Vogel, S. Goerres, K. Landfester, C. K. Weiss, *Macromol. Chem. Phys.* **2011**, *212*, 1719.
[51] X. H. Meng, D. Qiu, *Langmuir* **2014**, *30*, 3019.
[52] K. Shinotsuka, Y. Kajita, K. Hongo, Y. Hatta, *Langmuir* **2015**, *31*, 11452.

© 2018 WILEY-VCH Verlag GmbH & Co. KGaA, Weinheim